Cation Environment in Molten Lithium Iodide Doped Poly(ethylene oxide)

J. D. Londono,* B. K. Annis, and A. Habenschuss

Oak Ridge National Laboratory, Oak Ridge, Tennessee 37830

O. Borodin and G. D. Smith

Department of Chemical Engineering, University of Missouri-Columbia, Columbia, Missouri 65211

J. Z. Turner

Crystallography Department, Birkbeck College, London WC1E 7HX, U.K.

A. K. Soper

ISIS Science Division, Rutherford Appleton Laboratory, Chilton, Didcot, Oxon OX11-OQX, U.K.

Received April 24, 1997; Revised Manuscript Received September 11, 1997[⊗]

ABSTRACT: We present neutron diffraction isotopic substitution (NDIS) and molecular dynamics (MD) simulation results on molten poly(ethylene oxide) doped with LiI in a molar ratio of five ether oxygens per Li^+ ion. The NDIS and the MD studies yield estimates of the partial radial distribution function about the Li^+ ion. Using a quantum chemistry based atomistic force field, excellent agreement between simulation and experiment is obtained. The agreement between NDIS and MD is improved significantly if ion/ion and ion/polymer polarization effects are introduced in the simulations, indicating the importance of polarization effects in this system. Results indicate a strong coordination between the Li^+ cations and the ether oxygen atoms. The simulation results suggest a value of $n_O(r < 3\ \text{Å}) \simeq 3.5$ for the coordination number of oxygens about Li^+. The variation of n_O with Li−O separation to 2.5 Å is similar from simulation and experiment, although experimentally beyond 2.5 Å this function is impossible to determine.

Introduction

Poly(ethylene oxide)/alkali metal salt (PEO/M^+X^-) complexes have been investigated for over 30 years.[1] These complexes exhibit ionic conductivities[2] approaching that of many liquid electrolytes. The potential of these materials has been recognized[3] for use in anhydrous environments, and technological applications include solid-state batteries, fuel cells, and display devices. It is now accepted that the mechanism of ionic transport is greatly dependent on the cation environment.[3,4−6] Also, results indicate that the amorphous fraction of semicrystalline polymer electrolytes plays a major role in the conductivity,[7] because the crystalline regions of the polymer are an obstacle to ionic conduction.[8]

The structure of crystalline PEO/MX and oligomer/MX complexes has been the subject of several crystallographic studies [$PEO/LiCF_3SO_3$,[9] PEO/NaSCN,[10] heptaethylene glycol/$Sr(SCN)_2$,[11] PEO/NaI,[12] $PEO/NaClO_4$,[13] and $PEO/HgCl_2$[14]]. Valuable structural information has also been derived from spectroscopic studies of crystalline and noncrystalline samples of PEO/MX[15,16] and oligomer/MX[16,17] complexes. These studies[9−17] unanimously conclude that the conformation of the polymer chain changes upon complexation from the dominant C−O−C−C trans−trans−gauche (T_2G) conformation of high molecular weight PEO. This change in polymer conformation is indicative of strong specific interactions of the polymer with the ions.

The conformation of PEO molecules in the crystalline state has been well documented. For example, the structures of all 3:1 (EO:M, M = Li,[9] Na[10,12,13]) molar ratio crystalline complexes are very similar, with the metal ion being coordinated by three ether oxygens (EO), and the polymer chain adopting a 2/1 helix of conformation $T_2GT_2GT_2G'$, where G and G′ are plus and minus gauche bond conformations. Spectroscopic data[15] for a number of 4.5:1 (EO:M) complexes indicate that helical chains, of conformation (T_2GT_2G') slightly different from that of the 3:1 (EO:M) case, wrap around the cations. In this case, evidence suggests that four nearest neighbor oxygens are oriented toward the cation. In all of these cases the dominant interaction is the coordination of ether oxygen atoms to alkali metal cations, and it is reasonable to expect that this interaction will also be important in the amorphous phase.

The structure in the liquid or amorphous phase is much less clear. Spectroscopic results[16] indicate that the same conformational changes that occur in solid PEO upon complexation may also occur in liquid oligomer/salt complexes. In addition, the oligomer in the presence of salt may adopt a conformation that is energetically unfavorable in the pure liquid.[17] In this paper we investigate the atomic structure about the cation in the amorphous phase of a model polymer electrolyte. We present neutron diffraction isotopic substitution (NDIS) results, which yield a partial radial distribution function. This function describes the structure about the Li^+ ion in an amorphous sample of PEO/LiI of molar ratio 5:1. In addition, we have performed molecular dynamics (MD) simulations for comparison with the experimental results. A future paper will study the changes in conformation of the PEO chain on complexation in the amorphous phase.

Experimental Method

Two solutions, one containing ^{6}LiI and the other ^{nat}LiI in deuterated PEO ($[-CD_2-CD_2-O]_n$), were prepared in a dry-

[⊗] Abstract published in *Advance ACS Abstracts,* November 1, 1997.

S0024-9297(97)00568-8 CCC: $14.00

Table 1

element	atomic fraction	coeff in eq 8
O	0.135	0.124 (A/σ)
C	0.270	0.284 (B/σ)
D	0.541	0.572 (C/σ)
I	0.027	0.023 (D/σ)
Li	0.027	<0.001 (E/σ)

box. The d-PEO was obtained from Polymer Source Inc. (Quebec, Canada) and was prepared by anionic polymerization using (diphenylmethyl)potassium as an initiator. The M_n was 52k, the polydispersity was 1.06, and the deuteration level was greater than 99%. The ^{6}LiI (95.96% ^{6}Li) was obtained from Isotec (Miamisburg, OH). Typically, sample preparation proceeded as follows: PEO (≃2 g), LiI (≃1.2 g), and deuterated acetonitrile (12 g; H_2O content < 0.02% from NMR analysis) were weighed in a Teflon Petri dish and stirred at ≃80 °C on a hotplate for 1 h. The resultant slurry was subsequently transferred to a vacuum oven at 100 °C, where it remained overnight, reaching a final vacuum of ≃28 μmHg. The vacuum drying resulted in an amorphous solid. X-ray diffraction measurements ($Q_{max} = 16$ Å^{-1}) did not reveal any crystalline material at this concentration, which was taken as an indication of homogenous mixing. In particular, the X-ray measurements showed no evidence of crystalline LiI in the final solutions. The concentration of the solutions was 5:1 (EO:Li$^+$). Numerical values of atomic fraction are given in Table 1 for all the atomic species. Samples, 1.5 mm thick, were shaped in a press under vacuum and were loaded in flat plate cells between 1.5 mm thick windows ($Ti_{0.676}Zr_{0.324}$ zero coherent scattering alloy[18]) for the neutron scattering experiments.

Neutron scattering data were collected on the SANDALS[19] instrument at the ISIS pulsed neutron source (Rutherford Appleton Laboratory, U.K.) The measurements were performed at 90 °C. The number density, $\rho_a = 0.087$ Å^{-3}, was derived from neutron transmission measurements. Data were collected by the time-of-flight technique using 870 detectors ($3° < 2\theta < 32°$), but due to detector instabilities only 91% of the detectors generated useful data. Measurements were also made on empty containers, on a vanadium slab (3.5 mm thick), and of the background.

Simulation Method

Molecular dynamics (MD) simulations were performed on a model PEO/LiI system. Although simulation details have appeared elsewhere,[20−23] some salient features are given presently. The system consisted of 32 PEO chains composed of 12 repeat units (methyl terminated), with a LiI concentration corresponding to that employed in the scattering experiments (EO:Li$^+$ of 5:1). The simulations were performed, with periodic boundary conditions and at constant temperature and density, using the algorithm described previously.[20] The temperature and density of the model system corresponded to the parameters of the scattering experiments. A quantum chemistry based force field,[21] used in previous simulations of pure PEO melts,[22,23] was employed to describe the polymer/polymer interactions. The ion/ion and ion/polymer force field used was obtained from ab initio quantum chemistry studies of complexes of methane and model ethers with Li$^+$ and I$^-$ ions.[24] Ion/ion and ion/polymer polarization effects were described using a two-body polarization model, details of which have appeared elsewhere.[24,32] The effective ion and atomic polarizabilities were determined by fitting to quantum chemistry ion/ion and ion/ether complex energies.[24] Our quantum chemistry studies indicate that although electrostatic interactions are important in the binding of Li$^+$ ions to the model ether (primarily between the Li$^+$ and the ether oxygen atoms), about 50% of the binding in these complexes is the result of polarization effects. As in our previous simulations, we employed a distance dependent dielectric constant in treating electrostatic interactions[22,23] in the simulations of PEO/LiI. For polarization interactions, a distance dependent dielectric constant was also employed. Here, the dielectric constant had an onset distance of 4.5 Å and a bulk value of 50 (see ref 20 for a detailed description of the distance dependent dielectric constant). The system was equilibrated for approximately 1 ns or 10^6 time steps. Several sampling runs of up to 250 ps each were sufficient to obtain good statistics.

The length of the chains in the simulations were much longer than the statistical segment length[22] (SSL ≃ 6 Å) of PEO, which corresponds to an extended length (all-trans) of less than three repeat units. Beyond the SSL, intramolecular correlations are absent, and therefore monomer orientations are random. Thus, the model of oligomeric chains is expected to reproduce the short range correlations in polymeric chains as probed experimentally.

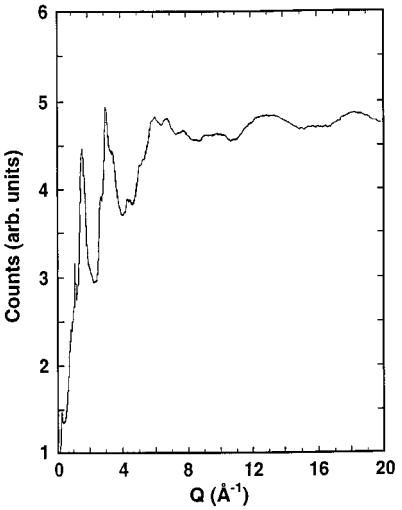

Figure 1. Neutron intensity (arbitrary units) as a function of Q for PEO/^{6}LiI prior to corrections and normalization.

Experimental Data Analysis

For ease of analysis the data were separated into 14 groups, each group being composed of detectors located within a narrow spread of scattering angles (2θ). Data from each group were corrected for background, multiple scattering, absorption, and empty can contributions, as described in the ATLAS data analysis manual.[25] The time of flight abscissa was converted to Q and, using the vanadium spectra, the ordinate intensity scale was normalized to absolute units (barn atom^{-1} sterad^{-1}), yielding the differential cross section $\Sigma(Q,2\theta)$. This quantity depends on 2θ and the momentum transfer Q ($=4\pi\lambda^{-1}\sin\theta$),[26,27]

$$\Sigma(Q,2\theta) = \sum_{\alpha} c_\alpha b_\alpha^2 \, \Sigma_i^s(Q,2\theta) + F(Q) \qquad (1)$$

where c_α and b_α are respectively the atomic fraction and scattering length, averaged over isotopic and spin states, of the atomic species α. The self-scattering cross-section given by the first term in eq 1 is affected by inelasticity effects, contained in the factor $\Sigma_i^s(Q,2\theta)$. The distinct or interference scattering cross-section, $F(Q)$, assumed to be unaffected by inelasticity effects,[28] carries the structural information of interest and is given by a weighted sum of the partial structure factors $S_{\alpha,\beta}(Q)$,

$$F(Q) = \sum_{\alpha,\beta} c_\alpha c_\beta b_\alpha b_\beta [S_{\alpha,\beta}(Q) - 1] \qquad (2)$$

Figure 1 shows data for one of the groups corresponding to PEO/^{6}LiI prior to the application of any corrections. The droop evident at $Q < 6$ Å^{-1} in the PEO/^{6}LiI data set is due to the increase in the absorption cross-section of the ^{6}Li isotope for low-energy neutrons. In Figure 2, an appropriately corrected and normalized PEO/^{6}LiI data set ($2\theta = 20°$) shows that the droop evident in the uncorrected data is absent, demonstrating

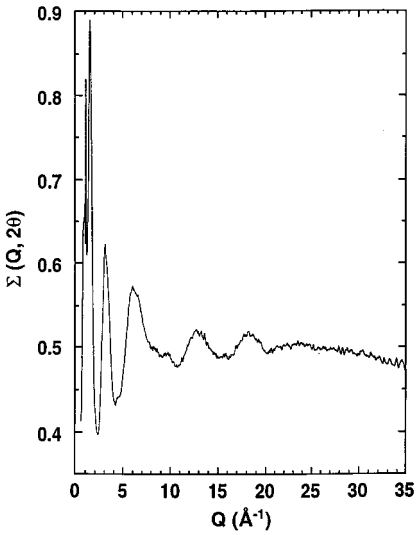

Figure 2. Differential scattering cross section for PEO/^{6}LiI at $2\theta = 20°$.

the suitability of the applied absorption and multiple scattering corrections.

The self-scattering cross-section term in eq 1 constitutes a smooth and slowly varying background on which the more rapidly varying $F(Q)$ term oscillates. The self-scattering term was approximated by fitting[29,30] to each of the 14 grouped data sets a second-order Chebyschev polynomial in $\ln[E(\lambda)]$, where $E(\lambda)$ is the neutron energy. The fitted polynomials were subsequently subtracted from the data sets, yielding $F(Q)$ for each group. A further low-frequency correction to $F(Q)$ was performed by setting to null the structure below $r = 0.5$ Å, after forward and subsequent back Fourier transformation to Q space. Finally, the groups were merged into a single data set spanning the range $0.2 \leq Q \leq 30$ Å^{-1}.

The partial pair correlation functions $g_{\alpha,\beta}(r)$ are related by Fourier inversion to their respective $S_{\alpha,\beta}(Q)$

$$S_{\alpha,\beta}(Q) = 1 + \frac{4\pi\rho_a}{Q}\int \mathrm{d}r\,[g_{\alpha,\beta}(r) - 1]r\,\sin(Qr)$$

$$g_{\alpha,\beta}(r) = 1 + \frac{1}{2\pi^2\rho_a r}\int \mathrm{d}Q\,[S_{\alpha,\beta}(Q) - 1]Q\,\sin(Qr) \quad (3)$$

The number of atoms of type β within a spherical shell of thickness dr at a distance r from a central atom of type α is given by

$$n_\beta(r) = 4\pi\rho_a c_\beta r^2 g_{\alpha\beta}(r)\,\mathrm{d}r \quad (4)$$

This expression was used to yield coordination numbers within specific ranges of distance via numerical integration.

The minimum noise (MIN) reconstruction[31] technique was used to Fourier transform the experimental Q-space functions. This is an iterative method, designed to produce an r-space function that is compatible with the input Q-space data and that is of minimum structure. Trial r-space functions were generated randomly, and these were compared with the input data after Fourier transformation. Moves were accepted or rejected on the basis of a quality factor, defined as the weighted sum of the residual (formally χ^2, difference of trial and input Q-space functions) and a measure of the noise in the trial r-space function. Further imposed conditions were that the result should be null below a prespecified distance (low r cutoff) and that it should be a positive

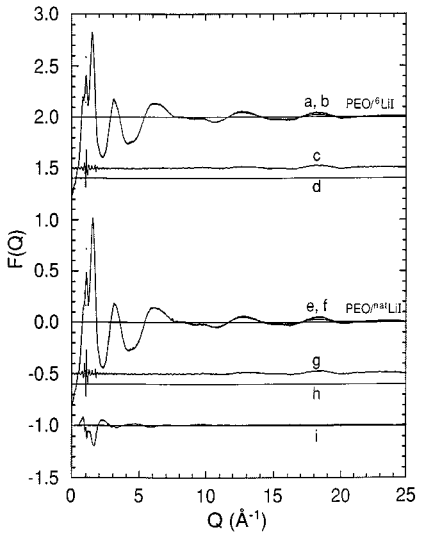

Figure 3. Interference scattering cross sections, $F(Q)$: (a) experimentally determined $F(Q)$ for PEO/^{6}LiI (+2.0); (b) output from MIN with associated errors superimposed (+2.0); (c) residual, obtained by subtracting the experimental from the MIN curve (+1.5); (d) experimental errors (+1.4). Identical information is shown in (e), (f), (g) (−0.5), and (h) (−0.6) for PEO/^{nat}LiI. (i) $F_{\mathrm{Li-6}}(Q) - F_{\mathrm{Li-Nat}}(Q)$ (−1.0).

function. Convergence was achieved when the quality factor was minimized. In addition, the quality of the result was assessed visually from the smoothness of the result and the lack of structure in the residual. In the MIN procedure, an ensemble of r-space functions are found to be compatible with the input data. The spread of this ensemble is shown as errors in Q- and r-space functions, and these are shown in addition to experimental errors in Q-space functions, which arise from counting statistics.

Results

Total Interference Function. Figure 3 shows for $F_{\mathrm{Li-Nat}}(Q)$ and $F_{\mathrm{Li-6}}(Q)$ the experimentally determined functions/errors and the MIN-related functions/errors and the residuals. Inspection of the residuals reveals that the MIN routine was unable to reproduce in both cases the sharp peak apparent in both data sets at ≃1.1 Å^{-1}. The presence of a sharp peak indicates the presence of some crystallinity in the samples. In order for MIN to reproduce this feature the transform (r-space function) should be extended to at least 200 Å, which is beyond the present implementation of the method. The fact that the sharp feature in $F(Q)$ was not reproduced by the MIN routine was of little consequence for the interpretation of the data. Apart from this discrepancy, the residuals show other features at $Q \simeq 15$ −20 Å^{-1}, which are of about the size of the experimental error bars. These features are due to the effects of the low r cutoff.

Figure 4 shows NDIS and MD results for $G(r)$. This is the function obtained from Fourier transformation of $F(Q)$, which comprises contributions from all of the atomic correlations in the system. Peaks corresponding to the following distances are discernible: C−H (≃1.1 Å), C−C and C−O (≃1.4−1.5), and first intrachain (1···3) nonbonded (C···O, C···C, etc. at ≃2.2−2.6 Å). The integral under the first experimental peak (≃1.1 Å) was found to be in good agreement with the expected two H atoms per carbon, demonstrating the appropriate scaling of the data. Both NDIS and MD agree in the overall pattern of the observed features, although there are minor disagreements in the height of the peaks, with

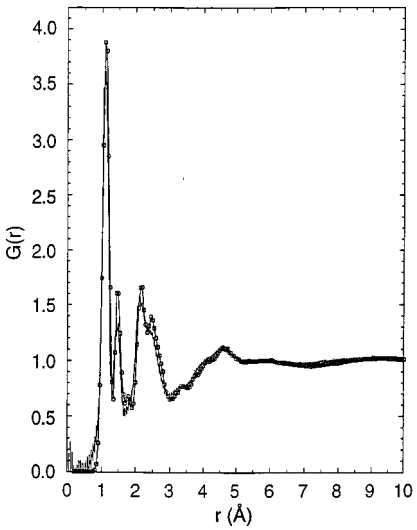

Figure 4. Total pair distribution function, $G(r)$, for PEO/^{6}LiI from MD (squares) and NDIS (line, with MIN errors superimposed).

the MD results being overall somewhat more "structured". In the MD model, stretching and bending force constants were scaled to account for quantum mechanical zero-point vibrational effects on the distribution of bond lengths and bond angles, and this scaling improved the agreement with experiment significantly.[32] Prior to scaling of the potential, simulation results displayed a prominent peak instead of a valley at 1.8 Å, corresponding to the shortest H···H intramolecular distance.

Difference Interference Function. The experimental $F(Q)$ results (Figure 3) for the two isotopically distinct solutions are very similar, and their difference is shown at the bottom of Figure 3. The difference is small due to the fact that the atom fraction of the isotopically substituted ion is also small (Table 1). One other factor that contributes to the size of the difference in $F(Q)$ is the scattering length difference between the two isotopic species ($b_{\mathrm{Li-Nat}} = -0.190 \times 10^{-14}$ m and $b_{\mathrm{Li-6}} = 0.2 \times 10^{-14}$ m[33]). The difference of the two $F(Q)$ functions contains information on the atomic structure about the isotopically substituted Li^+ ion. These concepts are developed in the following discussion.

If a pair of experiments are performed on PEO/MX samples which differ only in the isotopic state of the cation M, then the following difference may be formed,

$$\Delta F(Q) = \sigma^{-1}[F_M(Q) - F_{M'}(Q)]$$

$$= \sigma^{-1}\{A[S_{MO}(Q) - 1] + B[S_{MC}(Q) - 1] + C(S_{MD}(Q) - 1] + D[S_{MX}(Q) - 1] + E[S_{MM}(Q) - 1]\} \quad (5)$$

where, for example, the coefficient in the first term is given by

$$\frac{A}{\sigma} = \sigma^{-1} c_M c_O b_O (b_M - b_{M'})$$

$$\sigma = A + B + C + D + E \quad (6)$$

The direct space function $\Delta G(r)$, is obtained by Fourier inversion from $\Delta F(Q)$,

$$\Delta G(r) = 1 + \frac{1}{2\pi^2 \rho_a r} \int \mathrm{d}Q\, \Delta F(Q)\, Q \sin(Qr) \quad (7)$$

Although the function $\Delta G(r)$ depends only on all of those

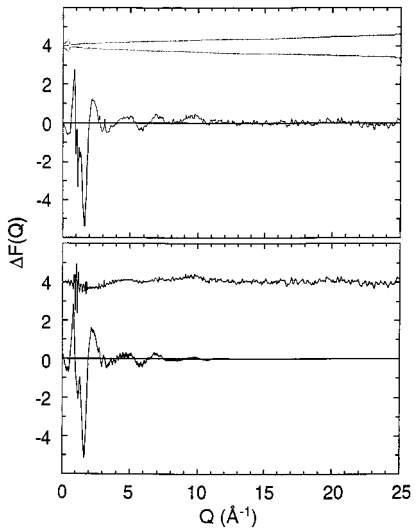

Figure 5. (Upper) $\Delta F(Q) = \sigma^{-1}[F_{\mathrm{Li-6}}(Q) - F_{\mathrm{Li-Nat}}(Q)]$. The envelope of the experimental errors is shown also (+4.0). (Lower) $\Delta F(Q)$ as output from MIN, with MIN errors superimposed. Residual is shown also (+4.0).

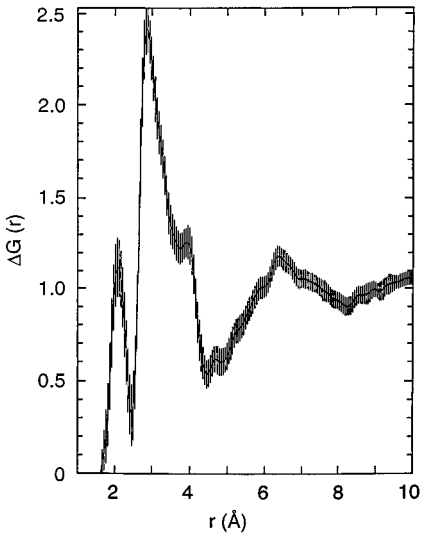

Figure 6. $\Delta G(r)$ with associated MIN errors.

$g_{\alpha,\beta}(r)$ that involve the M species, it depends primarily on the cation−polymer correlations, which are represented by the first three terms within the braces of the following expression, the other terms in eq 8 are negligible (see Table 1)

$$\Delta G(r) = 1 + \sigma^{-1}\{A[g_{MO} - 1] + B(g_{MC} - 1] + C[g_{MD} - 1] + D[g_{MX} - 1] + E[g_{MM} - 1]\} \quad (8)$$

The experimental $F(Q)$ functions were used to calculate $\Delta F(Q)$ according to eq 5 $\{\Delta F(Q) = \sigma^{-1}[F_{\mathrm{Li-6}}(Q) - F_{\mathrm{Li-Nat}}(Q)]\}$, and this function was used as input for the MIN routine. The experimental $\Delta F(Q)$ and the corresponding function as output by MIN are shown in Figure 5, in addition to experimental/MIN errors and the residual. The residual comprises low- and high-frequency components. The high-frequency components are extracted by the MIN routine as noise, while the low-frequency components are due to the low r cutoff $[\Delta G(r < 1.5\ \text{Å}) = 0]$, imposed on the data prior to back Fourier transformation to Q space. Figure 6 shows $\Delta G(r)$ obtained from Fourier transformation via the MIN procedure with associated MIN errors.

Li−X Structure: NDIS vs MD. A comparison of simulation and experimental results for $\Delta G(r)$ are

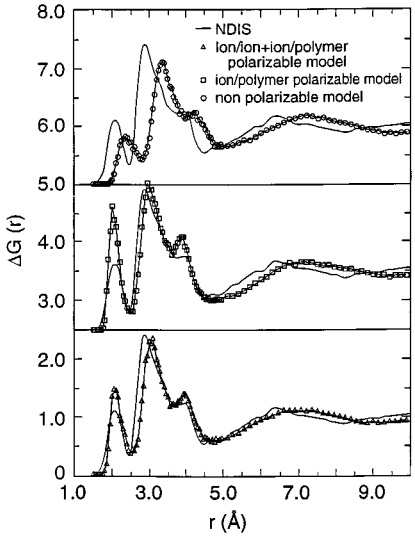

Figure 7. $\Delta G(r)$ from NDIS and MD. MD: polarizable model (triangles, +0.0); polarizable model without cation/anion polarization (squares, +2.5); nonpolarizable model (circles, +5.0). NDIS (full line, +0.0, +2.5, +5.0).

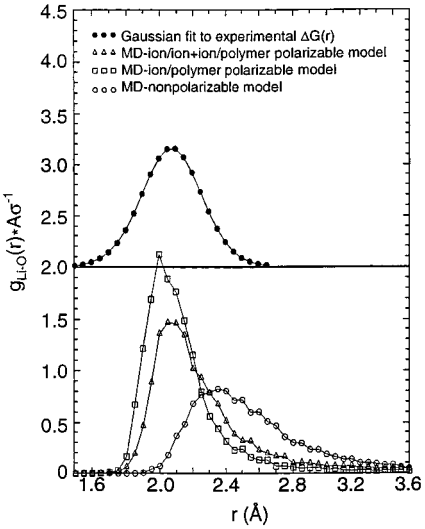

Figure 8. Li−O partial pair distribution function, $g_{Li^+-O}(r)$ from MD and NDIS. These functions are on the same scale as $\Delta G(r)$ (Figure 7) because $g_{Li^+-O}(r)$ has been multiplied by $A\sigma^{-1}$ (Table 1). MD: polarizable model (triangles); polarizable model without cation/anion polarization (squares); nonpolarizable model (circles). NDIS (filled circles, +2.0).

shown in Figure 7. Simulation results are shown for three force fields, which differ in the treatment of polarization effects. It is clear that for the nonpolarizable model, the calculated $\Delta G(r)$ deviates significantly from experiment. In this case all the peaks in the simulated $\Delta G(r)$ appear shifted to higher separations. This is particularly true for the first peak. When polarization effects are not included, the peak height is lower than experiment and occurs at a larger separation, indicating that the strength of the interactions between Li^+ and the polymer are underestimated.

Figure 8 shows the Li^+−O partial pair distribution functions as obtained from the simulations, and these results make it possible to clearly associate the first peak in the experimental $\Delta G(r)$ (Figure 7) at ≃2.1 Å with Li^+−O interactions. Figure 8 reveals that agreement with experiment improves for the first peak (Li^+−O) when polarization of the polymer by Li^+ and anion/anion polarization is taken into account. This is evidenced by a shift of the first peak toward smaller separations, matching the experimental results. However, in this case, the interactions between Li^+ and the polymer appear to be too strong: the peak height is greater, and subsequently the oxygen coordination number about Li^+ is larger than observed experimentally. Taking additionally the polarization effects between cation and anion into account resulted in a MD $\Delta G(r)$ function that matches well the NDIS curve in terms of peak height, width, and position. Inclusion of cation/anion polarization increases the strength of the Li^+−I^- interaction. As a result, more I^- anions were found in close proximity to the Li^+ cation. i.e., within the oxygen solvation radius of ≃3 Å. This is clearly demonstrated in Figure 9, which shows the coordination of I^- around Li^+, obtained from Li^+−I^- radial distribution functions integrated from zero to the radius r. Consequently, oxygen atoms are effectively displaced by I^- ions, resulting in a decrease in the height of the first peak in $\Delta G(r)$ (Figures 7 and 8). Note that there is no shift to larger separations of the first peak when cation/anion polarization effects are included, contrary to the shift observed when ion/polymer and anion/anion polarization effects were introduced to the nonpolarizable model.

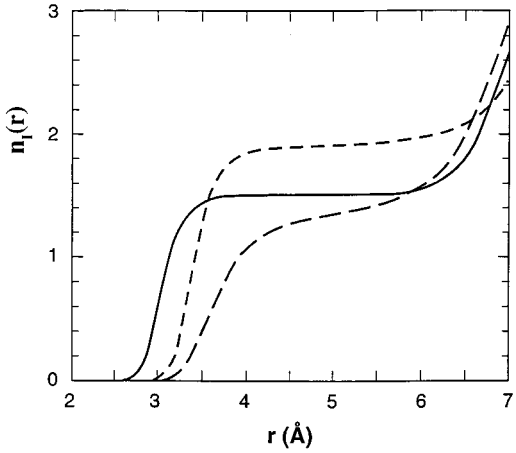

Figure 9. Number of I^- (n_I) within a sphere of radius r about a central Li^+ cation from MD simulations: (full line) polarizable model without cation/anion polarization; (short-dashed line) polarizable model; (dashed line) nonpolarizable model.

The MD Li^+−C and Li^+−H pair distribution functions are shown in Figure 10, and these results reveal that the second peak in $\Delta G(r)$ (Figure 7, $2.5 < r < 3.5$ Å) is due to Li^+−C and Li^+−H correlations. Within this range it is clear that agreement between MD and NDIS improves for the polarizable model even without cation/anion polarization over the nonpolarizable model (Figure 7). In addition, MD results for the second peak are less sensitive to cation/anion polarization effects than the first peak. The third peak ($r = 4$ Å), due to Li^+−H correlations, is better reproduced by the model that includes the cation/anion polarization effects. Further undulations are observed experimentally for $r > 4.5$ Å, and these are best matched when cation/anion polarization effects are taken into account in the MD calculations.

The experimental curve for $g_{Li^+-O}(r)$ as shown in Figure 8 constitutes an approximation, obtained by fitting the first peak in $\Delta G(r)$ with a Gaussian peak. The Gaussian shape fits well the experimental peak for $r < 2.3$ Å. At higher separations, overlap with the second feature in $\Delta G(r)$ precludes experimental determination of $g_{Li^+-O}(r > 2.3$ Å), and in this sense the Gaussian fit for $r > 2.3$ Å constitutes an extrapolation. This extrapolation is likely to be in error as the MD curves (polarization effects included) are small but

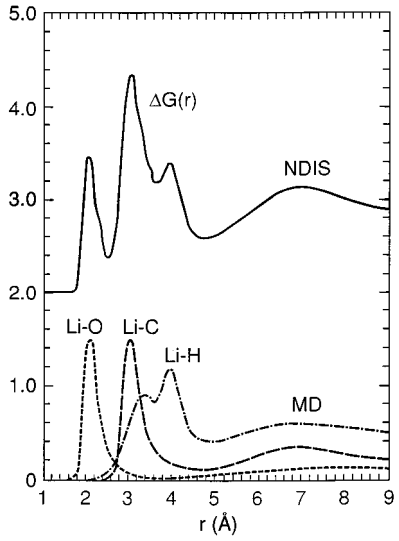

Figure 10. MD $\Delta G(r)$ (+2.0) and partial pair distribution functions of Li^+-O, Li^+-H, and Li^+-C correlations from the MD polarizable model. The partial pair distribution functions are scaled by the corresponding coefficients in eq 8, as given in Table 1. The sum of the scaled partials yields $\Delta G(r)$, neglecting the Li^+-I^- and Li^+-Li^+ contributions, which are small on this scale.

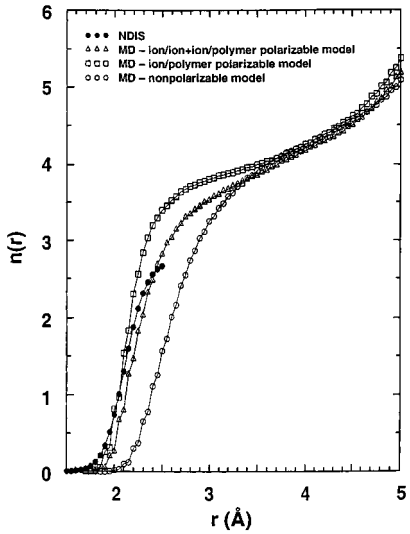

Figure 11. Number of O atoms about Li^+ within a sphere of radius r. MD: polarizable model (triangles); polarizable model without cation/anion polarization (squares); nonpolarizable model (circles). NDIS (filled circles).

nonzero for $r > 2.5$ Å, while the Gaussian approximation tends to zero in this range. In the following it is assumed that the error incurred in extrapolation is small for $r < 2.5$ Å.

The integrated pair distribution functions, which show the average number of oxygens within a sphere of a radius r about a central Li^+ ion (oxygen coordination number), are presented in Figure 11. Up to $r = 3$ Å the dependence of the oxygen coordination number on polarization effects is small: 3.3, 3.7, and 3.5 for the cases of no polarization, ion/ether + anion/anion polarization, and full polarization, respectively. We feel justified in choosing $r = 3$ Å as the cutoff in the calculation of the oxygen coordination number because the value of $g_{Li^+-O}(r = 3$ Å) is small compared to the peak height for the cases in which polarization is included (Figure 8). However, there are substantial differences beween the three MD curves in Figure 11 for $r < 3$ Å. The NDIS curve in Figure 10 was obtained by integration under the Gaussian curve presented in Figure 9. For separations up to $r = 2.5$ Å the experimental results clearly match more closely the MD results with polarization effects included. However, due to experimental uncertainties it is not possible to discriminate among the polarizable models on the basis of the coordination number results in Figure 10.

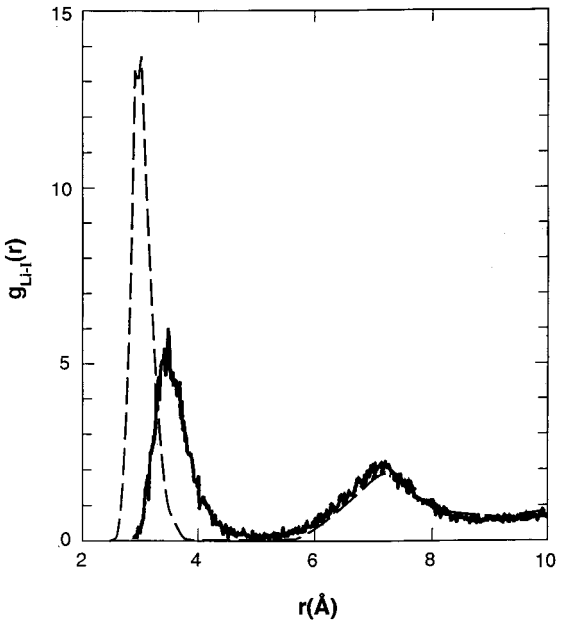

Figure 12. Li^+-I partial pair distribution function, $g_{Li^+-I}(r)$, from simulations: (dashed line) polarizable model; (full line) polarizable model without cation/anion polarization.

Ion Association. Examination of $\Delta G(r)$ from simulation (Figure 7) indicates that inclusion of cation/anion polarization effects improves agreement with experiment, particularly for the first (Li^+-O) peak. The polarization interaction in Li^+-I^- is about 50% of the Coulomb interaction at the equilibrium separation of 2.4 Å. As a consequence, we would expect to see more ion association (pairing and clustering) in the model, which includes cation/anion polarization. The temperature of the system investigated (90 °C) is well above the glass transition temperature of ≃10 °C determined from DSC scans (10 °C/min), and the salt concentration is rather high (EO:Li^+ of 5:1). For similar concentrations and temperatures, significant ion pairing/clustering was observed in such systems as $LiCF_3SO_3-PPO$ (poly(propylene oxide)) and $LiClO_4-PPO$ using Raman spectroscopy.[36–38] The function $g_{Li^+-I^-}(r)$ is presented in Figure 12 and shows that the cation/anion interaction has a strong effect on this function, giving rise to a sharp peak at 2.9 Å. Integration under this peak yields an estimate of about 1.4 I^- ions per Li^+ ion (Figure 9). More detailed statistics on ion pairing/clustering can be extracted from the MD results, and these are shown in Figure 13. For the fully polarizable model, Figure 13 shows that about 51% of Li^+ cations form aggregates with two I^- anions and just 4% of Li^+ form aggregates with three I^- atoms. Also formation of ion pairs (one I^- in the solvation shell of the Li^+) is rather probable, with 36% of the Li^+ participating in such complexes. Just 9% of all cations do not have any anions within the solvation sphere radius of 5 Å. Such cations might be considered as "free" cations. These concentrations of "free" cations, ion pairs, and ion aggregates are consistent with experimental observations for polymer salt systems at high temperatures and high salt concentration.[34–36] Note that "turning off" all polarization interactions increases the fraction of Li^+ cations participating in larger aggregates and decreases the

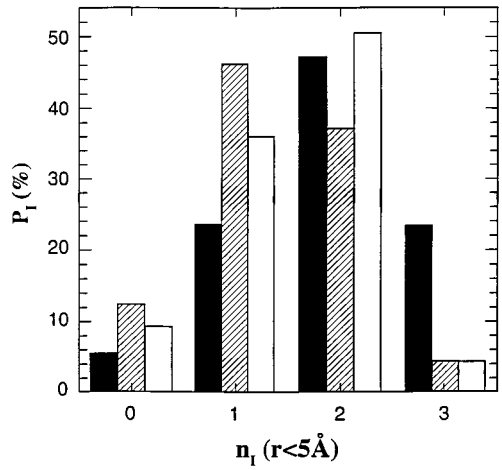

Figure 13. Probability of finding a certain number of I^- within a sphere of 5 Å from a central Li^+ cation (in percent), from MD simulations: (black) nonpolarizable model; (hash) polarizable model without cation/anion polarization; (white) polarizable model.

amount of "free" cations. This picture is consistent with a reduced solubility of LiI in PEO when polarization effects are neglected.

Conclusions

Both NDIS and MD results indicate that the atomic environment about the cation is highly structured, as it comprises a well-defined set of peaks. Such a highly structured environment is not unusual in aqueous solutions.[26] In other cases the solvation structure might be difficult to detect via NDIS.[37] In the present case of PEO/LiI, the structured environment about the cation is consistent with the reduced contribution of the cation to the conductivity with respect to the anion contribution and is also consistent with the higher activation energy necessary for ^{7}Li diffusion as compared to ^{19}F diffusion for PEO/$LiCF_3SO_3$.[38] These facts are in line with the accepted view that "the cation interacts more strongly with the PEO than the anion".[39]

The NDIS and MD results show that the first peak in $\Delta G(r)$ is at $\simeq$2.1 Å. This value is close to the average of the $Li^+\cdots$EO distances in the crystal structure of PEO/$LiCF_3SO_3$[9] and is in good agreement with the value obtained from quantum chemistry studies of Li^+ complexed by four dimethyl ether molecules in a tetrahedral arrangement.[24] The present results are therefore in agreement with the large body of work, referenced in the Introduction, that indicates that the dominant interaction in these systems is the coordination of ether oxygen atoms to alkali metal cations.

Our results suggest a value of $\simeq$3.5 for the coordination number of oxygens about Li^+. This value is difficult to specify because the Li^+-O distribution does not have a sharp cutoff, which might be due to diffusion of oxygens in and out of the Li^+ coordination shell. Interestingly, although the shape of the $g_{Li^+-O}(r)$ is strongly dependent on the way polarization is included, the coordination number is only moderately dependent. For example, when polarization is excluded, the Li^+-O distance increases significantly from that observed with the polarizable models, and the remaining Li^+-polymer pair distribution functions change radically, but the oxygen coordination number decreases by only 10−20%. Therefore, good agreement between simulation and experiment for the oxygen coordination number alone is not sufficient to indicate that a force field accurately describes the Li^+-polymer interaction.

References and Notes

(1) Yoshihara, T.; Tadokoro, H.; Murahashi, S. *J. Chem. Phys.* **1964**, *41*, 2902.
(2) Fenton, D. E.; Parker, J. M.; Wright, P. V. *Polymer* **1973**, *14*, 589. Wright, P. V. *Br. Polym. J.* **1975**, *7*, 319. Wright, P. V. *J. Polym. Sci., Polym. Phys. Ed.* **1976**, *14*, 955.
(3) Armand, M. B.; Chabagno, J. M.; Duclot, M. J. In *Fast Ion Transport in solids*; Vashishta, P., Mundy, J. N., Shenoy, G. K., Eds.; North Holland: New York, 1979; p 131.
(4) MacCallum, J. R.; Vincent, C. A. In *Polymer Electrolyte Reviews*; MacCallum, J. R., Vincent, C. A., Eds.; Elsevier: New York, 1987; Vol. 1, Chapter 2.
(5) Shriver, D. F.; Papke, B. L.; Ratner, M. A.; Dupon, R.; Wong, T.; Brodwin, M. *Solid State Ionics* **1981**, *5*, 83.
(6) Killis, A.; Le Nest, J. F.; Cheradame, H.; Gandini, A. *Makromol. Chem.* **1982**, *183*, 2835.
(7) Davis, G. T.; Chaing C. K. *High Ionic Conduction in Polymers (Kinosei Kobunshi Zairyo)*; CMC: Tokyo, 1984.
(8) LeNest, J. F.; Gandini, A.; Schoenenberger, C. *Trends Polym. Sci.* **1994**, *2*, 432.
(9) Lightfoot, P.; Mehta, M. A.; Bruce, P. G. *Science* **1993**, *262*, 883.
(10) Chatani, Y.; Fujii, Y.; Takayanagi, T.; Honma, A. *Polymer* **1990**, *31*, 2238.
(11) Ohmoto, H.; Kai, Y.; Yasuoka, N.; Kasai, N. *Bull. Chem. Soc. Jpn.* **1979**, *52*, 1209.
(12) Chatani, Y.; Okamura, S. *Polymer* **1987**, *28*, 1815.
(13) Lightfoot, P.; Mehta, M. A.; Bruce, P. G. *J. Mater. Chem.* **1992**, *2*, 379.
(14) Iwamoto, R.; Saito, Y.; Ishihara, H.; Tadokoro, H. *J. Polym. Sci., Polym. Phys. Ed.* **1968**, part A2 vol *6*, 1509−1525. Yokoyama, M.; Ishihara, H.; Iwamoto, R.; Tadokoro, H. *Macromolecules* **1969**, *2*, 184.
(15) Papke, B. L.; Ratner, M. A.; Shriver, D. F. J. *Phys. Chem. Solids* **1981**, *42*, 493.
(16) Frech, R.; Huang, W. *Macromolecules* **1995**, *28*, 1246.
(17) Frech, R.; Huang, W. *Solid State Ionics* **1994**, *72*, 103.
(18) Sidhu, S. S.; Heaton, L.; Zauberis D. D.; Campos, F. P. *J. Appl. Phys.* **1956**, *27*, 1040.
(19) Soper, A. K. In *Advanced Neutron Sources 1988*; Hyer, D. K., Ed.; IOP Conference Series No. 97; IOP: Bristol, PA, 1989.
(20) Smith, G. D.; Jaffe, R. L.; Yoon, D. Y. *Macromolecules* **1993**, *26*, 298.
(21) Smith, G. D.; Jaffe, R. L.; Yoon, D. Y. *J. Phys. Chem.* **1993**, *97*, 12752.
(22) Smith, G. D.; Yoon, D. Y.; Jaffe, R. L.; Colby, R. H.; Krishnamoorti, R. *Macromolecules* **1996**, *29*, 3462.
(23) Smith, G. D.; Yoon, D. Y.; Wade, C. G.; O'Leary, D.; Chen, A.; Jaffe, R. L. *Macromolecules*, in press.
(24) Smith, G. D.; Jaffe, R. L.; Partridge, H. *J. Chem. Phys.* **1997**, *101*, 1705.
(25) Soper, A. K.; Howells, W. S.; Hannon, A. C. Rutherford Appleton Laboratory Report No. RAL-89-046, 1989.
(26) Nielson, G. W.; Enderby, J. E. *Proc. R. Soc. London* **1983**, *A390*, 353.
(27) Postorino, P.; Ricci, M. A.; Soper, A. K. *J. Chem. Phys.* **1994**, *101*, 4123.
(28) Placzek, G. *Phys. Rev.* **1952**, *86*, 377.
(29) Andreani, C.; Merlo, V.; Ricci, M. A.; Soper, A. K. *Mol. Phys.* **1991**, *73*, 407.
(30) Andreani, C.; Nardone, M.; Ricci F. P.; Soper, A. K. *Phys. Rev.* **1992**, *A46*, 4709.
(31) Soper, A. K. In *Neutron Scattering Data Analysis 1990*; Johnson M. W., Ed.; IOP Conference Series No. 107; IOP: Bristol, PA, 1990; pp 57−67.
(32) Smith, G. D.; Borodin, O.; Pekny, M.; Annis, B.; Londono, D.; Jaffe, R. L. *Spectrochim. Acta* **1997**, *A53*, 1273.
(33) Sears, V. F. Atomic Energy of Canada Limited internal report (AECL-8490), Chalk River, Ontario, 1984.
(34) Kakihana, M.; Schantz, S.; Torell, L. M. *J. Chem. Phys.* **1990**, *92*, 6271.
(35) Bernson, A.; Lindgren, J. *Solid State Ionics* **1993**, *60*, 37.
(36) Schants, S. *J. Chem. Phys.* **1991**, *94*, 6296.
(37) Bieze, T. W. N.; Barnes, A. C.; Huige, C. J. M.; Enderby, J. E.; Leyte, J. C. *J. Phys. Chem.* **1994**, *98*, 6568.
(38) Bhattacharja, S.; Smart, S. W.; Whitmore, D. H. *Solid State Ionics* **1986**, *45*, 261.
(39) Ward, I. M.; Boden, N.; Cruickshank, J.; Leng, S. A. *Electrochim. Acta* **1995**, *40*, 2071.

MA9705681